

# Four-wavelength Ultra-narrow Linewidth Fiber Laser enabled by a Figure-8 Compound-ring-cavity Filter and a Polarization-managed Four-channel Filter

Ting Feng, *Member, OSA*, Da Wei, Wenwen Bi, Weiwei Sun, Shengbao Wu, Meili Jiang, Fengping Yan, Yuping Suo and X. Steve Yao, *Fellow, IEEE, Fellow, OSA*

**Abstract**—We propose and demonstrate a high performance four-wavelength erbium-doped fiber laser (4W-EDFL), enabled by a figure-8 compound-ring-cavity (F8-CRC) filter for single-longitudinal-mode (SLM) selection and a polarization-managed four-channel filter (PM-FCF) for defining lasing wavelengths. We introduce a novel methodology utilizing signal-flow graph combined with Mason’s rule to analyze a CRC filter in general and apply it to obtain the important design parameters for the F8-CRC filter used in this paper. By combining the functions of the F8-CRC filter and the PM-FCF filter assisted by the enhanced polarization hole-burning and polarization dependent loss, we achieve the 4W-EDFL with fifteen lasing states, including four single-, six dual-, four tri- and one quad-wavelength lasing operations. In particular, all the four single-wavelength operations are in stable SLM oscillation, typically with a linewidth of  $<600$  Hz, a RIN of  $\leq -154.58$  dB/Hz@ $\geq 3$  MHz and an output power fluctuation of  $\pm 3.45\%$ . In addition, all the six dual-wavelength operations have very similar performances, with the performance parameters close to those of the single-wavelength lasing operations. Finally, we achieve the wavelength spacing tuning of the dual-wavelength operations for the photonic generation of tunable microwave signals, and successfully obtain a signal at 23.10 GHz as a demonstration.

**Index Terms**—Fiber laser, figure-8 compound-ring-cavity filter, polarization-managed four-channel filter, ultra-narrow linewidth.

## I. INTRODUCTION

SINGLE-longitudinal-mode (SLM) erbium-doped fiber laser (EDFL) in C-band (1530 nm~1565 nm) has been adopted

This work was supported by the National Natural Science Foundation of China under Grant 61975049, 61775128 and 12004092, and the Hebei Provincial Natural Science Foundation for Outstanding Young Scholars under Grant F2020201001. (*Corresponding author: X. Steve Yao.*)

T. Feng, D. Wei, W. Bi, W. Sun, S. Wu and M. Jiang are with the Photonics Information Innovation Center, Hebei Provincial Center for Optical Sensing Innovations, Hebei University, Baoding 071002, China (e-mail: wlxyft@hbu.edu.cn; weida0328@163.com; bww1998@163.com; sunweiwei\_888@163.com; swu@hbu.edu.cn; jiangmeili@enn.cn).

F. Yan is with the Institute of Lightwave Technology, Beijing Jiaotong University, Beijing 100044, China (e-mail: fpyan@bjtu.edu.cn).

Y. Suo is with the Shanxi Provincial People’s Hospital, Shanxi Medical University, Taiyuan 030012, China (e-mail: ypsuo@sxmu.edu.cn).

X. S. Yao is with the Photonics Information Innovation Center, Hebei University, Baoding 071002, China, and is also with the NuVision Photonics, Inc., Las Vegas, NV 89109, USA (e-mail: steveyao888@hbu.edu.cn).

or anticipated as the preferred light source for many important applications, due to its outstanding inherent merits such as low intensity and phase noise, narrow linewidth, high beam quality, and excellent compatibility with fiber optical systems. Narrow linewidth single-wavelength EDFLs with high stability have been utilized commercially or tested experimentally in the cutting-edge applications such as ultra-long distance coherent optical communication, coherent fiber optic sensing, high resolution optical metrology and spectroscopy, and coherent Doppler LiDAR [1-5]. They are also promising in the potential applications relating to optical atomic clocks, measurements of fundamental constants and physics [6, 7]. A multi-wavelength EDFL (MW-EDFL), with a narrow linewidth SLM operation for every lasing wavelength, is strongly desired as the light source in the areas such as photonic generation of high spectral purity microwave signals, multi-parameter optical fiber sensing, and wavelength division multiplexing fiber systems in the future [8-12]. Therefore, it is attractive to achieve flexible switching among single- and multi-wavelength operations in a single SLM EDFL system. Generally, a switchable MW-EDFL with stable SLM oscillation for every lasing line involves the following key techniques: I) SLM selection, II) multi-channel filter to define the primary lasing wavelengths, III) switching mechanism to control the operation mode, and IV) mechanism to stabilize the multi-wavelength lasing.

Ultra-short distributed feedback and distributed Bragg reflector (DBR) oscillating structures are the easiest and most mature methods to achieve SLM operation for a fiber laser [13-16]. However, the limited output power, low flexibility and difficulty for achieving multi-wavelength operation are the major shortcomings. A long oscillating cavity with an ultra-narrow filter to obtain the SLM operation is another main method [17, 18]. However, the severe spatial-hole-burning induced by the standing-wave effect in gain fibers, leading to an unstable SLM lasing, cannot be avoided in the DBR based and other linear cavities. In contrast, a long ring structure with an ultra-narrow filter is a preferable scheme for the SLM EDFL, especially for a switchable MW-EDFL. Commonly available ultra-narrow optical filters include the high finesse Fabry-Pérot (F-P) etalon [19] and the fiber Bragg grating (FBG) based filters, such as phase-shifted FBG [20], FBG-based F-P filter

[21], and chirped moiré FBG [22], but they are all complicated or expensive. Compound-ring-cavity (CRC) made of several cascaded or nested fiber rings is a low-cost and easy alternative to obtain high-quality ultra-narrow filters, which has been verified by our group [23-26] and others [27-30]. In the previous work [24], we designed a dual-coupler ring based compound-cavity (DCR-CC) filter with a passband of  $\sim 8.20$  MHz and a free spectrum range of  $\sim 10.22$  GHz, which has an excellent SLM selection capability and is made with four fiber optical couplers (OCs) with a very low cost of  $< 20$  US dollars. In this paper, we present a even lower cost and more compact CRC filter, named figure-8 CRC (F8-CRC) filter made of only 3 OCs. This F8-CRC also has the superb capability to enable SLM oscillating for the proposed four-wavelength EDFL (4W-EDFL) reported in this paper. Furthermore, in this work, we introduce a new efficient analysis methodology for the CRC filters dedicated to SLM fiber lasers in general.

There are numerous multi-channel filters proposed for defining primary lasing wavelengths in MW-EDFLs [22, 23, 25, 31-45]. Multiple wavelength-switch mechanisms have been successfully used, such as those based on polarization control [22, 24, 25, 34, 39, 40], nonlinear polarization rotation (NPR) [36, 37], intensity-dependent inhomogeneous loss [46], and tunable-filter scanning [33]. Additionally, to suppress the wavelength competition induced by the homogenous broadening effect of rare-earth doped gain fibers to stabilize the multi-wavelength lasing, the mechanisms involving the NPR based or nonlinear amplifier loop mirror based amplitude equalizer [25, 47], four-wave mixing [48-50], and polarization-hole-burning (PHB) [23, 24, 44] are reported in literatures. Among the proposed techniques, the polarization control is an excellent way to achieve the switching among different operation states of MW-EDFLs, especially combining it with a polarization dependent multi-channel filter, such as a high-birefringence FBG (HB-FBG) [23]. The HB-FBG, with two narrowband reflection channels, can be fabricated in a segment of polarization maintaining fiber (PMF). Meanwhile, the use of the HB-FBG in a laser cavity can introduce the enhanced PHB effect in the gain fiber [23], which can mitigate the wavelength competition significantly to obtain stable dual-wavelength operation. In the previous work [24], we designed a four-channel superimposed HB-FBG (SI-HB-FBG) reflecting filter, and used it in a 4W-EDFL to achieve the switch operation among 15 lasing states, including single-, dual-, tri- and quad-wavelength operations. However, since the lasers reflected from channel-1 and channel-3, channel-2 and channel-4 of the SI-HB-FBG were respectively with the same state of polarization (SOP), the switching among multi-wavelength operations were a bit difficult and the fluctuations of the two lasers simultaneously oscillating with same SOP were larger than the two lasers with orthogonal SOPs. In order to resolve these issues, in this work, we propose a novel design to fusion splice two HB-FBGs together with a  $45^\circ$  polarization-axial-offset to form a novel polarization-managed four-channel filter (PM-FCF), in which the reflected lights from four channels all have different SOPs. In addition, using the SI-HB-FBG as a four-channel filter in the 4W-EDFL

[24], the spacing between any two channels of which cannot be changed. However, using the PM-FCF, the wavelength spacing between different channels of two HB-FBGs can be changed by stretching one of the HB-FBGs while keeping the other one static. To date, there is only one report on a four-channel filter made of two cascaded HB-FBGs for achieving a switchable multi-wavelength fiber laser [51], however the authors used a polarization controller (PC) between two HB-FBGs to rotate the polarization. Not only their approach is complicated and unstable, but also has the issue that the laser outputs are all not in SLM oscillation. To the best of our knowledge, a PM-FCF made of two HB-FBGs fusion spliced together with a  $45^\circ$  polarization-axial-offset has not yet been reported.

In this paper, we introduce a F8-CRC filter and a PM-FCF in a ring cavity fiber laser as enabling components for SLM selection and for defining lasing wavelengths, respectively, both for the first time. With the aids of the two components, we achieve a high performance 4W-EDFL, capable of switching among fifteen output states, including four single-, six dual-, four tri- and one quad-wavelength operations. Specifically, we first introduce a novel methodology utilizing the signal-flow graph combined with the Mason's rule to analyze a CRC filter in general, and apply it to obtain the important design parameters for the F8-CRC filter. The expected F8-CRC filter is fabricated successfully with the designed parameters. Next, we use the strong PHB effect introduced mainly by the PM-FCF to mitigate wavelength competition. We then control the SOPs to bring polarization dependent loss (PDL) for different lasers, and finally achieve the switchable multi-wavelength operations with high stability. As part of the demonstration, we show that, in all four single- and six dual-wavelength operations, the 4W-EDFL exhibits superb performances in terms of spectrum stability, optical signal to noise ratio (OSNR), SLM, mode-hopping, linewidth, power fluctuation, relative intensity noise (RIN) and polarization characteristics. We also demonstrate the capability of the 4W-EDFL for the photonic generation of tunable microwave signals. Finally, the superiority for tri- and quad-wavelength switchable operations based on the PM-FCF is validated and analyzed, in comparison with what can be achieved with the SI-HB-FBGs.

## II. EXPERIMENTAL SETUP, PRINCIPLES AND THEORY

### A. Laser Configuration

Figure 1 shows the schematic diagram of the proposed 4W-EDFL, which is a typical ring-cavity structure, simply composed of a novel PM-FCF, a novel F8-CRC filter and few other components.  $\sim 2.9$  m long EDF (Fibercore M12-980-125), coiled around the plates of a three-loop PC (TL-PC), is pumped by a commercial 980 nm laser diode (LD, Connet VLSS-980) through a 980/1550 nm wavelength division multiplexer (WDM). The reflecting PM-FCF, composed of two cascaded HB-FBGs, HB-FBG1 and HB-FBG2, fusion spliced together with a  $45^\circ$  polarization-axial-offset between each other, is innovatively used for defining the four lasing wavelengths. A three-port optical circulator is used to ensure the unidirectional

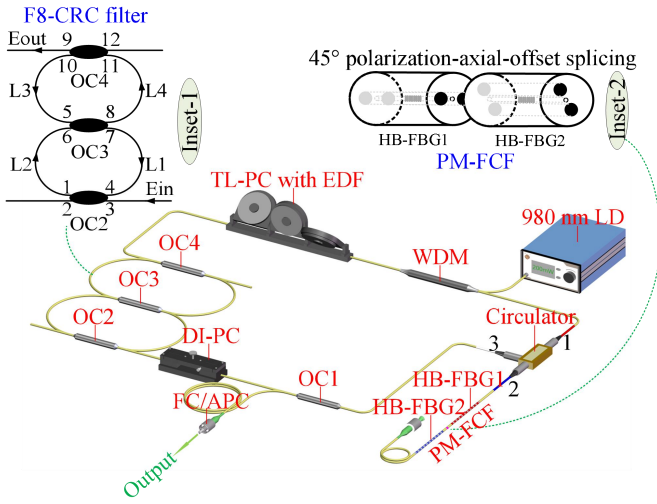


Fig. 1. Configuration of the proposed 4W-EDFL system. LD, laser diode; WDM, wavelength division multiplexer; TL-PC, three-loop polarization controller; EDF, erbium-doped fiber; OC, optical coupler; DI-PC, drop-in polarization controller; HB-FBG, high-birefringence fiber Bragg grating; F8-CRC, figure-8 compound-ring-cavity; PM-FCF, polarization-managed four-channel filter. The TL-PC made with a length of 2.9 m EDF pigtailed by single-mode fibers (SMF-28) at both sides; Inset-1 showing the components of the F8-CRC filter, where L1~L4 denoting lengths of fibers and 1~12 denoting port numbers of OCs; Inset-2 illustrating the 45° polarization-axial-offset fusion splicing of PMF pigtails of HB-FBG1 and HB-FBG2, composing the PM-FCF. An FC/APC connector used behind the PM-FCF to avoid the unnecessary reflections.

propagation of light. A drop-in polarization controller (DI-PC), combining with the TL-PC, can adjust the SOP of light in the laser cavity to balance the gains and losses of oscillating lasers. The F8-CRC filter, made of three OCs (OC2, OC3 and OC4), is employed to select one expected mode from the dense longitudinal-modes of the main-ring cavity (MRC). The laser is finally extracted from the 10% port of another OC (OC1 with a cross-coupling-ratio of 90:10) to be measured and utilized. The length of the MRC measured by a tape-measure is ~18.25 m, determining a longitudinal-mode spacing of ~11.17 MHz.

The HB-FBG1 and HB-FBG2 were fabricated respectively using the phase mask method [23, 24, 33, 52] in a section of hydrogen-loaded Panda-type PMF (YOFC, PM#1550\_125). The ultraviolet (UV) light at 248 nm emitting from a KrF excimer laser was used as the grating writing light source. A uniform phase mask with a period of 1075 nm and a length of 130 mm was used. The lengths of two HB-FBGs were both 100 mm. Due to the different effective refractive index between the slow and fast axes of the high-birefringence PMF, one HB-FBG exhibits two reflection channels, corresponding to two orthogonal linear polarization modes at the two polarization-axes. Note that, in order to provide different reflection channels for HB-FBG1 and HB-FBG2, compared to the writing of HB-FBG2, a suitable extra tensile-force was imposed to the PMF before the HB-FBG1 was written. That was equal to using two uniform phase masks with different periods to write two gratings in turn. Therefore, in theory the PM-FCF filter was expected to have four reflection channels. The pure reflection optical spectrum of the PM-FCF, measured using an optical spectrum analyzer (OSA, Yokogawa

AQ6370D) with a non-polarized light from a customized EDF amplifier (EDFA) on the basis of the measurement method described in [24], is shown in Fig. 2(a) in normalized linear scale. The resolution and data sampling interval of the OSA were 0.02 nm and 0.001 nm respectively.

It is worth noting that, since the PM-FCF are polarization dependent, the reflectivities of 36.09%, 36.97%, 37.57% and 38.05% for four channels (CH1, CH2, CH3 and CH4), as marked in Fig. 2(a) measured using the non-polarized light, are not real for a linearly polarized light input into the gratings. In order to measure the real reflectivity of each channel and verify the success of 45° polarization-axial-offset splicing between two HB-FBGs, we measured the pure reflection spectrum of the PM-FCF with a SOP controlled broadband light, based on the measurement method shown in Fig. 2(b). Four steps from (i) to (iv) as described in the caption of Fig. 2 were carried out. Compared to the non-polarized measurement method [24], an extra in-line fiber polarizer (POL) and an extra PC (the other TL-PC) were used. By adjusting the SOP of the polarized light input the PM-FCF using the PC, a maximal reflectivity for CH1, CH2, CH3 and CH4 was measured in turn using the experimental setup illustrated in step (i), when the polarization direction of input light was paralleling with the polarization-axis of CH1, CH2, CH3 and CH4, respectively. Then, through eliminating the effects of EDFA, POL, circulator and PC after finishing the measurements of steps (ii) ~ (iv), the pure reflection spectrum for each channel was obtained. The measured four pure reflection spectra are shown in Fig. 2(b) to Fig. 2(e), respectively.

As can be seen from Fig. 2(c) to Fig. 2(f), the real reflectivities of four polarization-dependent channels are 69.50%, 70.96%, 72.91% and 73.08% respectively. Taking the Fig. 2(b) as an example, as expected, we see that the reflectivity of CH2 measured is almost zero when the SOP of input light is paralleling to the polarization-axis of CH1. That is because the polarization-axes of CH1 and CH2 are orthogonal. In addition, we see that the reflectivities of CH3 and CH4 are close to half of that of CH1, since the polarization-axes of CH3 and CH4 are respectively 45° and 135° orientation with respect to that of CH1, as illustrated as the coordinate system. The similar situations are seen in Fig. 2(d) to Fig. 2(f), and on the basis of the results we know that the 45° polarization-axial-offset splicing between HB-FBG1 and HB-FBG2 is guaranteed. Note that the measured reflectivities in Fig. 2(d)~Fig. 2(f) may contain some errors resulting from the limited polarization extinction ratio (PER) of the POL, inaccuracy of manually adjusting the PC and the little fusion splicing loss between the PMF and single-mode fiber (SMF). Four channels are centered at 1556.666 nm, 1557.327 nm, 1558.138 nm and 1558.795 nm, respectively, with full-widths at half maximum (FWHMs) of 0.153 nm, 0.153 nm, 0.139 nm and 0.153 nm. The narrow FWHMs enable the PM-FCF to be a good reflection filter for the 4W-EDFL. The FWHMs can be narrowed further by using another PMF with higher photo-sensitivity, extending the writing length of grating, and further optimizing the writing parameters including the UV laser power, the focus position and moving speed of the light spot. In addition, the first two

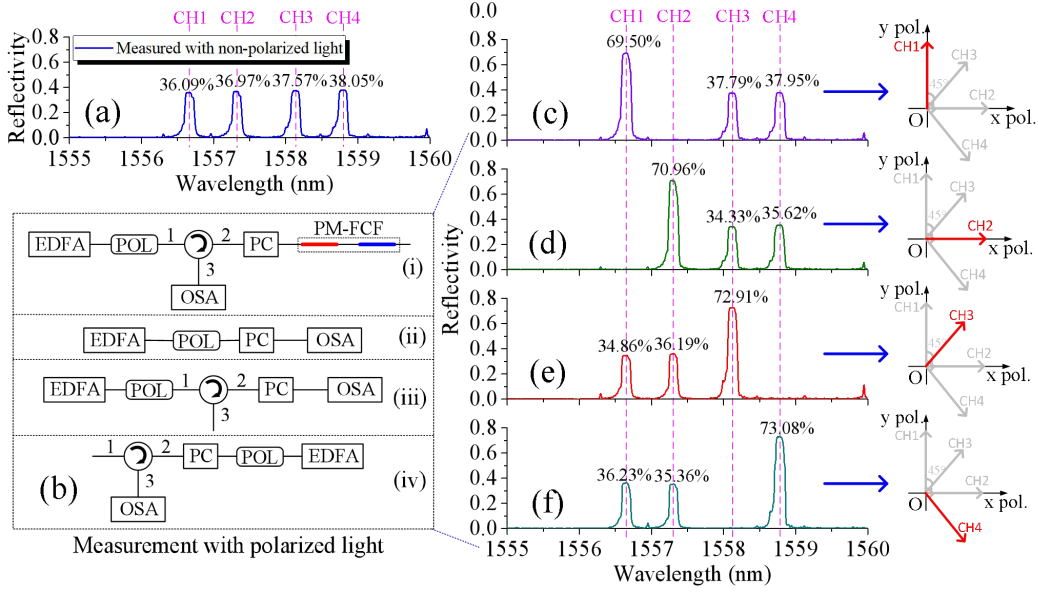


Fig. 2. (a) Pure reflection spectrum of PM-FCF in normalized linear scale measured with non-polarized light using the method described in Ref. [24]. (b) Measurement method of pure reflection spectrum of PM-FCF with polarized light, including procedures: (i) measurement of reflection spectrum of PM-FCF involving loss spectra of POL, port 1 to port 2 and port 2 to port 3 of circulator both and PC, and effect of output spectrum of EDFA; (ii) measurement of output spectrum of EDFA with the loss spectra of POL and PC; (iii) measurement of output spectrum of EDFA involving loss spectra of POL, port 1 to port 2 of circulator and PC; (iv) measurement of output spectrum of EDFA involving loss spectra of POL, PC and port 2 to port 3 of circulator. Pure reflection spectra of PM-FCF measured with polarized light, the SOP of which paralleling with the polarization-axis of (b) CH1, (c) CH2, (d) CH3 and (e) CH4, respectively. EDFA, EDF amplifier; POL, polarizer; PC, polarization controller; OSA, optical spectrum analyzer; CH1, CH2, CH3 and CH4, four reflection channels of PM-FCF.

reflection channels and the last two reflection channels are respectively with a spacing  $\Delta\lambda$  of 0.661 nm and 0.657 nm, corresponding to a birefringence  $\Delta n$  of  $\sim 6.14 \times 10^{-4}$ , calculated using the equation  $\Delta\lambda = \Delta n \cdot \Lambda$  ( $\Lambda = 1075$  nm is the period of phase mask), which is consistent with the value for PMF in 1550 nm band. Note that the birefringence could be changed to some extent by the high pressure hydrogen-loading process compared to that measured by the manufacturer before the PMF leaves the factory.

### B. Study on F8-CRC Filter for SLM Operation of Proposed 4W-EDFL

The F8-CRC filter used in the proposed fiber laser, as shown in Fig. 1, is assembled by three  $2 \times 2$  fiber OCs (OC2, OC3 and OC4). We set 1~12 and  $E_1 \sim E_{12}$  as the light ports of the OCs and the corresponding electric-field amplitudes respectively,  $\kappa_i$  ( $i = 2, 3, 4$ ) and  $\gamma_i$  ( $i = 2, 3, 4$ ) as the cross-coupling ratio and insertion loss of the  $i$ th OC respectively,  $L_1 \sim L_4$  as the fiber lengths,  $\alpha$  as the fiber loss coefficient,  $\delta$  as the fusion splicing loss, and  $\beta = 2\pi n_{eff} / \lambda$  as the light propagation constant.

Where,  $n_{eff}$  is the effective refractive index and  $\lambda$  is the light wavelength. The F8-CRC can be represented in a signal-flow graph [53, 54], as shown in Fig. 3. Twelve optical ports of OCs are represented as photonics nodes and eleven of them, 1~11, are involved in Fig. 3. In order to analyze the optical filtering performance or transitive relation from node 3 ( $E_{in}: E_3$ ) to node 9 ( $E_{out}: E_9$ ) using Mason's rule [53, 54] expressed as Eq. 1, we need to analyze the dependence of eleven nodes among each other and the path and loop gains of signal-flows firstly, based

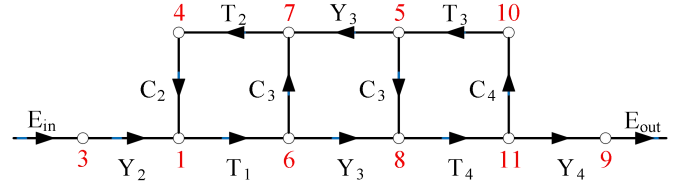


Fig. 3. Signal-flow graph representation of the F8-CRC filter.

on the signal-flow graph in Fig. 3.

$$H = \frac{1}{\Delta} \sum_i P_i \Delta_i, \quad (1)$$

where,  $H$  is the network function relating an input and an output port, and  $P_i$  is the gain of the  $i$ th forward optical path from  $E_{in}$  to  $E_{out}$ . The  $\Delta$  denotes the determinant of the signal-flow graph, given as

$$\Delta = 1 - \sum_i Q_i + \sum_{l \neq m} Q_l Q_m - \sum_{l \neq m \neq n} Q_l Q_m Q_n + \dots, \quad (2)$$

where  $\sum_i Q_i$  is the sum of all loop gains,  $\sum_{l \neq m} Q_l Q_m$  is the sum of products of all loop gains of two non-touching optical loops, and  $\sum_{l \neq m \neq n} Q_l Q_m Q_n$  is the sum of products of all loop gains of three non-touching optical loops.  $\Delta_i$  in Eq. (1) denotes the determinant  $\Delta$  after all loops that touch the path  $P_i$  at any node have been eliminated.

As shown in Fig. 3, we define the straight transmittance  $C_i$

of three OCs as

$$C_i = \sqrt{1-\gamma_i} \sqrt{1-\kappa_i} \quad (i = 2, 3, 4), \quad (3)$$

the cross-coupling transmittance  $Y_i$  of three OCs as

$$Y_i = i\sqrt{\kappa_i} \sqrt{1-\gamma_i} \quad (i = 2, 3, 4), \quad (4)$$

and the propagating gain  $T_i$  of fiber optical paths  $L_i$  as

$$\begin{cases} T_1 = \sqrt{1-\delta} e^{(-\alpha+j\beta)L_1} \\ T_2 = \sqrt{1-\delta} e^{(-\alpha+j\beta)L_2} \\ T_3 = \sqrt{1-\delta} e^{(-\alpha+j\beta)L_3} \\ T_4 = \sqrt{1-\delta} e^{(-\alpha+j\beta)L_4} \end{cases}. \quad (5)$$

There are 3 loops in Fig. 3, respectively involving the optical nodes 1-6-7-4-1, 8-11-10-5-8, and 1-6-8-11-10-5-7-4-1, and the propagating gain  $Q_i$  can be given by

$$\begin{cases} Q_1 = T_1 C_3 T_2 C_2 \\ Q_2 = T_4 C_4 T_3 C_3 \\ Q_3 = T_1 Y_3 T_4 C_4 T_3 Y_3 T_2 C_2 \end{cases}. \quad (6)$$

As can be seen,  $Q_1$  and  $Q_2$  are from two non-touching optical loops. So, according to Eq. (2), the determinant  $\Delta$  can be expressed as

$$\Delta = 1 - (Q_1 + Q_2 + Q_3) + Q_1 Q_2. \quad (7)$$

Only one forward optical path from  $E_{in}$  to  $E_{out}$ , involving the nodes 3-1-6-8-11-9, can be found in Fig. 3, and the propagating gain  $P_1$  of which can be given as

$$P_1 = Y_2 T_1 Y_3 T_4 Y_4. \quad (8)$$

According to Eq. (2), the corresponding  $\Delta_i$  can be known as

$$\Delta_i = 1. \quad (9)$$

Therefore, based on the Mason's rule, the transmission function  $H$  from  $E_{in}$  to  $E_{out}$  can be obtained as

$$H = \frac{E_9}{E_3} = \frac{P_1 \Delta_1}{\Delta}. \quad (10)$$

Subsequently, the transmittance  $T$  of the F8-CRC filter can be derived from Eq. (3)~Eq.(10), and is expressed as Eq. (11), where the parameters  $x$ ,  $y$  and  $z$  are given as

$$T = \frac{E_9}{E_3} \cdot \left( \frac{E_9}{E_3} \right)^* = \frac{\kappa_2 \kappa_3 \kappa_4 (1-\gamma_2)(1-\gamma_3)(1-\gamma_4)(1-\delta)^2 e^{-2\alpha(L_1+L_4)}}{1+x^2+y^2+z^2-2(x+yz)\cos[\beta(L_1+L_2)]-2(y+xz)\cos[\beta(L_3+L_4)]+2xy\cos[\beta(L_1+L_2-L_3-L_4)]+2z\cos[\beta L]} \quad (11)$$

$$\begin{cases} x = \sqrt{1-\gamma_2} \sqrt{1-\gamma_3} \sqrt{1-\kappa_2} \sqrt{1-\kappa_3} (1-\delta) e^{-\alpha(L_1+L_2)} \\ y = \sqrt{1-\gamma_3} \sqrt{1-\gamma_4} \sqrt{1-\kappa_3} \sqrt{1-\kappa_4} (1-\delta) e^{-\alpha(L_3+L_4)} \\ z = \sqrt{1-\gamma_2} \sqrt{1-\gamma_4} \sqrt{1-\kappa_2} \sqrt{1-\kappa_4} (1-\gamma_3) (1-\delta)^2 e^{-\alpha L} \\ L = L_1 + L_2 + L_3 + L_4 \end{cases} \quad (12)$$

Based on the theory above, we can simulate the transmission spectrum of the F8-CRC filter, and then, by combining the measured reflection spectrum of the PM-FCF, we can design the fabrication parameters for the F8-CRC filter aiming for selecting one longitudinal-mode from dense modes in the MRC of the proposed EDFL. According to our previous study [24], for a ring fiber laser with a FBG as the initial lasing wavelength decider and an ultra-narrow comb filter as the SLM selector, the free spectrum range (FSR) and passband of the comb filter must be larger than 0.5 times of the FBG's reflection bandwidth and less than 2 times of the MRC's mode-spacing of the fiber laser, respectively. The FWHM for every reflection peak of the PM-FCF is  $\sim 0.15$  nm measured, corresponding to a frequency range of  $\sim 18$  GHz, and the mode-spacing of the MRC is calculated to be  $\sim 11.17$  MHz. By comprehensively considering the theory, transmittance, feasibility and handwork tolerance of fabrication for the F8-CRC filter and after optimizing the simulations, we decided the parameters as  $L_1 = L_3 = L_4 = 0.25$  m,  $L_2 = 0.27$  m,  $\kappa_i (i = 2, 3, 4) = 0.05$ ,  $\alpha = 0.2$  dB/km,  $\delta = 0.01$  dB,  $\gamma_i (i = 2, 3, 4) = 0.09$  dB and  $n_{eff} = 1.468$ . The simulated transmission spectrum of the F8-CRC filter is shown as the blue solid-line in Fig. 4(a), and the measured reflection spectrum of the PM-FCF is also plotted using the red dashed-line. As can be seen, the FSR of the F8-CRC filter is 10.20 GHz and only one transmission peak is located in the FWHM of every channel of the PM-FCF. Multiplying the two curves in Fig. 4(a) by each other, we obtain the combined filtering effect of the F8-CRC filter and the PM-FCF, as shown in Fig. 4(b). Four narrow channels are seen and expected to be utilized to achieve wavelength-switchable lasing in the 4W-EDFL. By zooming in to see the maximum transmission peak in the third channel as shown in the inset-1 of Fig. 4(b), there are two passbands both with a 3-dB bandwidth as narrow as  $\sim 8.75$  MHz, which allows only one longitudinal-mode to pass through.

Based on the simulation parameters above, we fabricated the F8-CRC filter using three commercial OCs all with a coupling ratio of 95:5, trying our best to minimize the handwork error. Then, placing it on a common metal optical table, we measured its transmission spectrum under room temperature, by inputting a sweeping-laser from a wavelength-swept laser source (Yenista T100S-HP) into the filter and detecting its output

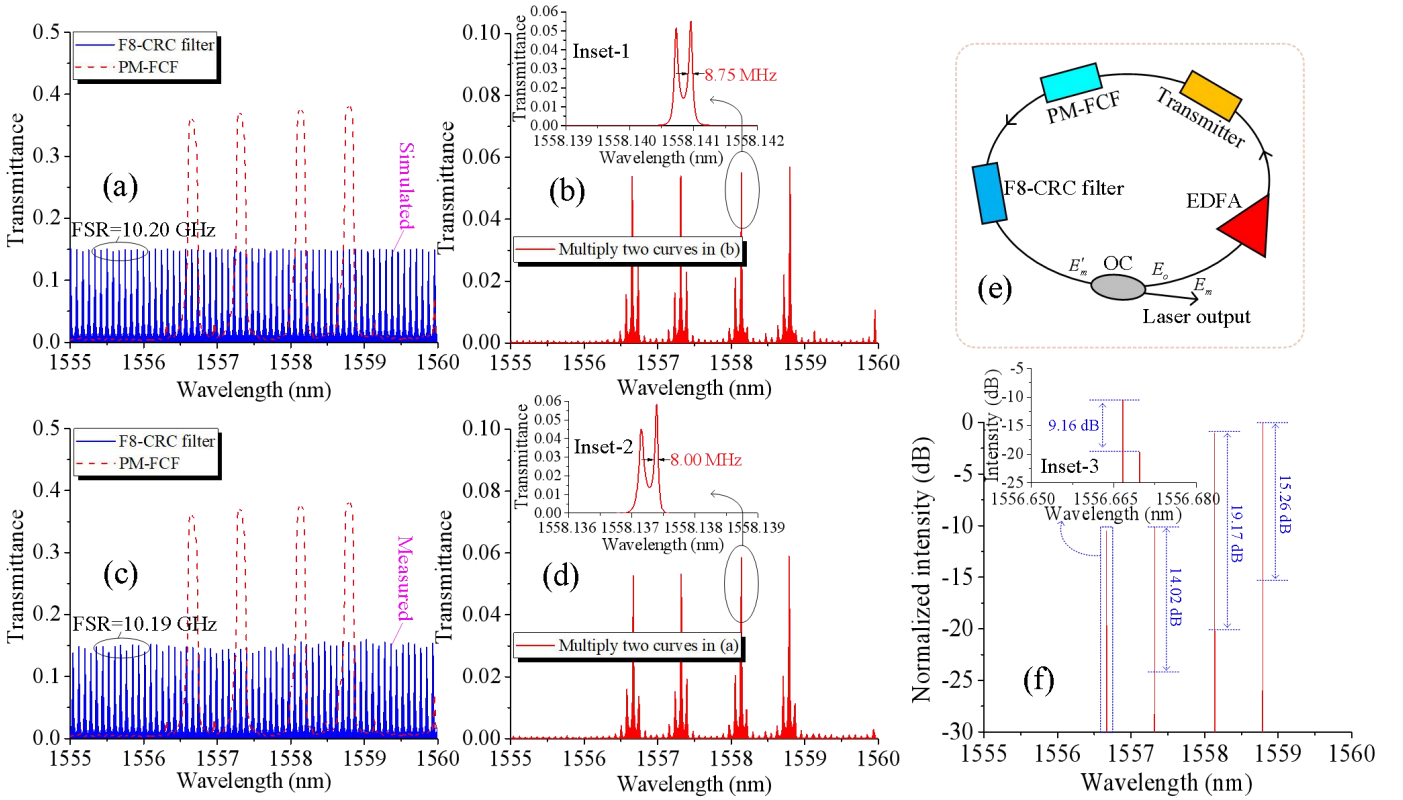


Fig. 4. (a) Simulated transmission spectrum of F8-CRC filter plotted by blue solid-line, with measured reflection spectrum of PM-FCF plotted by red dashed-line for comparison; (b) Combined filtering effect of F8-CRC filter and PM-FCF obtained by multiplying two curves in (a); Inset-1 showing the enlarged maximum transmission peak in the third channel in (b). (c) Measured transmission spectrum of F8-CRC filter plotted by blue solid-line, with measured reflection spectrum of PM-FCF plotted by red dashed-line for comparison; (d) Combined filtering effect of F8-CRC filter and PM-FCF obtained by multiplying two curves in (c); Inset-2 showing the enlarged maximum transmission peak in the third channel in (d). (e) Simple ring EDFL model for verifying the capability of F8-CRC filter combining with the PM-FCF to select SLM theoretically; (f) Simulated laser oscillating for 20 loops for the model in (e) but without considering the gain saturation effect and homogeneous broadening effect induced mode competition in the EDF; Inset-3 showing the enlarged laser oscillating in the first channel in (f).

using a 400 MHz photodetector (PD, Thorlabs PDB470C). The photovoltage of the PD was monitored by a data acquisition card (DAQ, Measurement Computing Cor. USB-1602HS). The laser source was with a sweeping-speed of 1 nm/s and a sweeping-range of 1554~1561 nm, and the DAQ was with a data sampling rate of 500 kHz. In the data processing, the laser wavelength vs. data sampling interval and the laser power vs. PD's photovoltage were calibrated each other, respectively. Figure 4(c) plots the measured result using the blue solid-line and also plots the reflection spectrum of the PM-FCF using the red dashed-line. As can be seen, the experimental result in Fig. 4(c) is in good agreement with the corresponding simulated spectrum of the F8-CRC filter in Fig. 4(a), and the measured FSR of 10.19 GHz is very close to the simulated value of 10.20 GHz. Figure 4(d) gives the combined filtering effect of the F8-CRC filter and the PM-FCF based on measured curves in Fig. 4(c), using the same data processing method to obtain Fig. 4(b). And also, high consistency is seen between the simulated and measured results respectively shown in Fig. 4(b) and Fig. 4(d). The measured passband of 8.00 MHz shown in the inset-2 of Fig. 4(d) is close to that of 8.75 MHz seen in the inset-1 of Fig. 4(b). All in all, the high consistency between simulation and experiment validates that our research approach for CRC filter is with high feasibility and accuracy. The little

inconsistency is mainly from the parameter errors of coupling ratios and insertion losses of commercial OCs, fusion splicing losses and fiber lengths in the filter fabrication with them used in the simulations.

To verify the capability of our F8-CRC filter combining with the PM-FCF to select SLM in a fiber laser theoretically, we build a simple ring EDFL model as shown in Fig. 4(e). In that, an EDF amplifier (EDFA) is introduced as the gain medium, the F8-CRC filter and the PM-FCF are both abstracted to transmission filters, an OC with a coupling ratio of 90:10 outputs the laser from the 10% port, a transmitter used represents the total loss including the extra insertion losses of above components and the passive fiber loss. We define the transmission functions of the F8-CRC filter and the PM-FCF as  $T_{CRC}$  and  $T_{FBG}$  respectively, and subsequently the combined transmittance given in Fig. 4(d) is exact the  $T_{CRC}T_{FBG}$ . Here, we introduce a small signal gain  $G$  for the EDFA, and assume that the loss value of the transmitter is  $A$ . Then, for a small signal with an amplitude of  $E_o$  oscillating inside the laser cavity for  $m$  loops, the laser amplitude  $E'_m$  can be given as

$$\begin{aligned}
E'_m &= E_o \sqrt{G} \sqrt{A} \sqrt{T_{CRC} T_{FBG}} e^{(-\alpha L + j\beta L_c)} + \\
&\quad \left[ E_o \sqrt{G} \sqrt{A} \sqrt{T_{CRC} T_{FBG}} e^{(-\alpha L + j\beta L_c)} \right] \cdot q + \\
&\quad \left[ E_o \sqrt{G} \sqrt{A} \sqrt{T_{CRC} T_{FBG}} e^{(-\alpha L + j\beta L_c)} \right] \cdot q^2 + \dots + \dots \quad (13) \\
&\quad \left[ E_o \sqrt{G} \sqrt{A} \sqrt{T_{CRC} T_{FBG}} e^{(-\alpha L + j\beta L_c)} \right] \cdot q^m \\
&= \frac{\left[ E_o \sqrt{G} \sqrt{A} \sqrt{T_{CRC} T_{FBG}} e^{(-\alpha L + j\beta L_c)} \right] (1 - q^m)}{1 - q}
\end{aligned}$$

Where  $L_c$  denotes the laser cavity length, and the factor  $q$  is given as

$$q = \sqrt{G} \sqrt{A} \sqrt{T_{CRC} T_{FBG}} \sqrt{1 - \kappa} e^{(-\alpha L + j\beta L_c)}. \quad (14)$$

Then the output amplitude from the OC can be obtained as

$$\begin{aligned}
E_m &= \sqrt{\kappa} \cdot E'_m \\
&= \sqrt{\kappa} \cdot \frac{\left[ E_o \sqrt{G} \sqrt{A} \sqrt{T_{CRC} T_{FBG}} e^{(-\alpha L + j\beta L_c)} \right] (1 - q^m)}{1 - q}, \quad (15)
\end{aligned}$$

where  $\kappa$  is the cross-coupling ratio of the OC. Finally, the simulated laser output from the cavity can be derived from Eq. (13)~(15) as

$$\begin{aligned}
I_{out} &= E_m \cdot E_m^* \\
&= \frac{E_o^2 q^2 \kappa \left[ 1 - 2 \left( q e^{-j\beta L_c} \right)^m \cos(\beta L_c m) + \left( q e^{-j\beta L_c} \right)^{2m} \right]}{(1 - \kappa) \left[ e^{2j\beta L_c} - 2q \cos(\beta L) e^{j\beta L_c} + q^2 \right]}, \quad (16)
\end{aligned}$$

Please note that in the simple modeling above, we ignore both the gain saturation effect presented in the practical EDFA and the mode competition induced by the homogeneous broadening effect presented in the practical EDF. So, it is reasonable that the laser output intensity will be infinity for an infinite number of oscillating loops, as can be inferred from Eq. (15).

Based on the laser model above, we assume that  $G = 20$  dB,  $A = -5$  dB,  $L_c = 18.257$  m same with that of the experimental laser cavity, and  $\kappa = 0.1$ , and then for a typical number of oscillating loops  $m = 20$  the laser output can be calculated as shown in Fig. 4(f). As can be seen, four lasing lines with side-mode suppression ratios (SMSRs) of 9.16 dB (as marked in inset-3), 14.02 dB, 19.17 dB and 15.26 dB respectively are obtained, corresponding to the four channels of the PM-FCF. Note that the intensity labeled in the y-axis of Fig. 4(f) is normalized to one using the maximum of the four main peaks and is converted into decibel. Considering that in the EDF there is strong homogeneous broadening induced mode competition effect, a SMSR of  $>9.16$  dB can definitely enable the SLM lasing in each channel of the PM-FCF theoretically. Therefore, the fabricated F8-CRC filter combing with the PM-FCF is able to achieve SLM operation for the proposed 4W-EDFL in all four channels in theory.

### C. Principles of Wavelength-switchable Operation

The EDF is a typical homogenous broadening gain medium,

so generally under room temperature severe mode/wavelength competition is presented inside the pumped EDF for an EDFL. In addition, for the 4W-EDFL shown in Fig. 1, since each channel's reflectivity of the PM-FCF is strong polarization dependent, so the loss of an oscillating laser at any channel can be easily controlled by adjusting the DI-PC and the TL-PC carefully. That is the major part of PDL inside the laser cavity. On the basis of above two aspects, one can make the lasing at an expected wavelength suffer lowest loss, and consequently the proposed 4W-EDFL can easily achieve single-wavelength switching-operation among four wavelengths theoretically. However, one cannot achieve stable simultaneously oscillating of several wavelengths through only controlling the PDL to suppress the severe wavelength competition in an EDFL cavity. In the proposed 4W-EDFL, we introduced the PHB effect for achieving multi-wavelength operation. The PHB in an EDF arises from the randomly distributed orientations of erbium ions in the glass matrix and the selective deexcitation of those ions aroused by a polarized light [55]. The lights reflected by the PM-FCF with different SOPs can utilize different subsets of excited erbium ions, indicating that the gains of the lights with different SOPs are contributed by different groups of ions. That can mitigate the wavelength competition significantly. As aforementioned, the PM-FCF is made of two HB-FBGs fusion spliced together with a  $45^\circ$  polarization-axial-offset and can reflect four wavelengths all with different linear SOPs. So they can be amplified by the different excited erbium ions. In addition, the gain EDF coiled around the three circular plates of the TL-PC can introduce slight stress inside itself and therefore a birefringence which depends on the radius of the EDF and the radius of the plates [44]. In the coiled EDF, the orientations of the polarization axes depend on the angular orientations of the three plates, meaning that a rotation of the plates will rotate the two polarization axes. Therefore, by tuning the TL-PC, the polarization axes of the coiled EDF can be aligned with the polarization directions of the incident lights at different wavelengths. Also, the output SOPs from the TL-PC can be controlled to well match with the expected channels' SOPs of the PM-FCF. Then the net gains at the expected reflection wavelengths of the PM-FCF are almost equal, which further enhances the PHB effect inside the laser cavity. Finally, the expected wavelengths experience the same small-signal gain and achieve lasing simultaneously with high stability.

## III. EXPERIMENTAL RESULTS AND DISCUSSION

The proposed 4W-EDFL system was constructed and deployed on an ordinary steel optical table, and we carried out all experiments under laboratory room temperature (with constant temperature air conditioning) without employing any vibration isolation and temperature compensation techniques. When the pump power of 980 nm LD was beyond the lasing threshold of the 4W-EDFL, we achieved fifteen lasing states, including one single-, six dual-, four tri- and four quad-wavelength operations through adjusting the TL-PC and DI-PC carefully to tune the polarization-axes of the coiled EDF and the SOP of light inside the laser cavity. We emphasized to study the lasing characteristics of single- and dual-wavelength

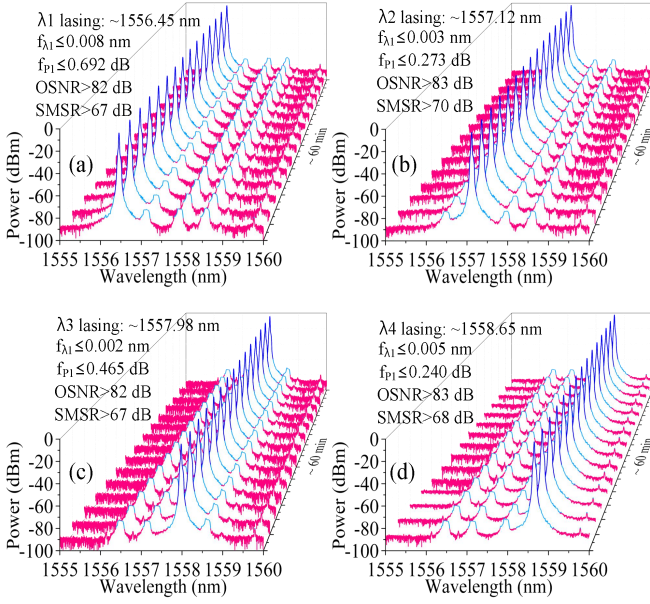


Fig. 5. Spectra of single-wavelength switchable operations lasing at (a)  $\lambda_1$ , (b)  $\lambda_2$ , (c)  $\lambda_3$  and (d)  $\lambda_4$ , respectively, measured in a time span of  $\sim 60$  min.  $f_{\lambda_i}$  ( $i=1, 2, 3, 4$ ): fluctuation of wavelength lasing at  $\lambda_i$ ;  $f_{p_i}$  ( $i=1, 2, 3, 4$ ): fluctuation of power lasing at  $\lambda_i$ ; OSNR: optical signal to noise ratio; SMSR: side-mode suppression ratio. In each figure 15 repeated spectra measured by OSA with an interval of  $\sim 4$  min.

operations and the photonic generation of microwave signal with the dual-wavelength lasing output of the 4W-EDFL.

#### A. Single-Wavelength Operation

Using a pump power of 200 mW for demonstration, we obtained stable single-wavelength operations lasing at  $\lambda_1$ ,  $\lambda_2$ ,  $\lambda_3$  and  $\lambda_4$  respectively, as shown in Fig. 5(a) to Fig. 5(d). The switching among four wavelength operations was implemented through adjusting the two PCs inside the laser cavity carefully. In each graph of Fig. 5, 15 repeated optical spectrum scanings were measured in a time span of  $\sim 60$  min, by the AQ6370D OSA using a resolution of 0.02 nm and a data sampling interval of 0.001 nm, to demonstrate the lasing stability of the 4W-EDFL. As can be seen in each graph, we gives the key parameters extracted from the three-dimensional (3-D) curves. The four lasers are with little to no wavelength fluctuation  $f_{\lambda_i}$  ( $i=1, 2, 3, 4$ ) (Maximum: 0.008 nm, less than the resolution of OSA) and low power fluctuation  $f_{p_i}$  (Maximum: 0.692 dB) lasing at  $\lambda_i$  ( $i=1, 2, 3, 4$ ). Note that the lasers respectively concentrated at  $\sim 1556.45$  nm ( $\lambda_1$ ),  $\sim 1557.12$  nm ( $\lambda_2$ ),  $\sim 1557.98$  nm ( $\lambda_3$ ) and  $\sim 1558.65$  nm ( $\lambda_4$ ) are basically consistency with the center wavelengths of the PM-FCF' four channels. We believe that the little wavelength deviation and the slight instability aforementioned were mainly induced by the additional force from the fixation of PM-FCF, the fluctuation of ambient temperature, the RIN of pump LD and the inevitable vibrations of surroundings. In addition, the OSNRs are all higher than 82 dB and the SMSRs are all larger than 67 dB for the four lasers, indicating that the laser cavity design is excellent with a high quality factor.

The longitudinal-mode characteristics of the 4W-EDFL at each lasing wavelength were firstly investigated by a scanning

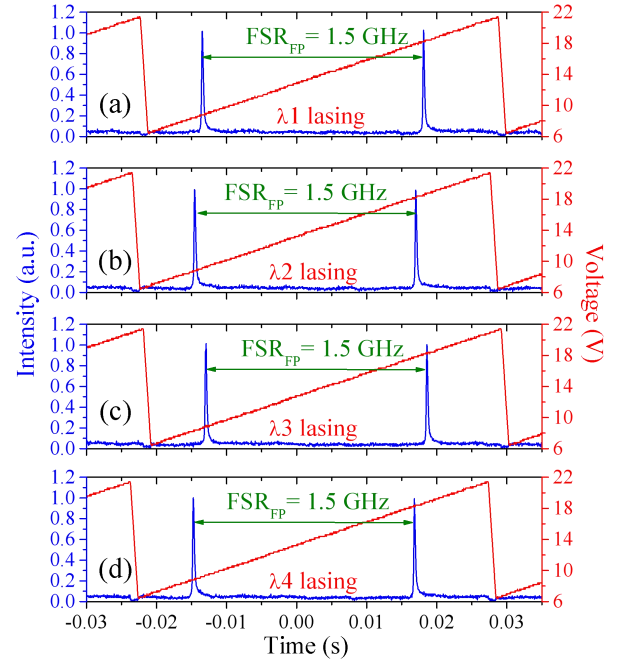


Fig. 6. Longitudinal-mode characteristics, measured by a scanning Fabry-Pérot interferometer, in single-wavelength operation lasing at (a)  $\lambda_1$ , (b)  $\lambda_2$ , (c)  $\lambda_3$  and (d)  $\lambda_4$ , respectively.

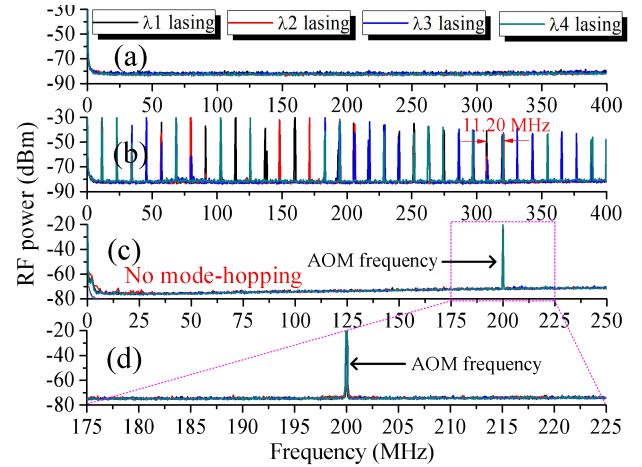


Fig. 7. RF spectra measured by ESA for all single-wavelength operations in turn, with different colored curves for different lasing wavelengths. (a) Self-homodyne RF spectra measured in a range of 0–400 MHz using maximum-hold (MH) mode of ESA in  $\sim 10$  min with resolution bandwidth (RBW) of 51 kHz. (b) Self-homodyne RF spectra measured in a range of 0–400 MHz using MH mode of ESA in  $\sim 10$  min with RBW of 51 kHz when F8-CRC filter replaced by SMF with a same length. Delayed self-heterodyne RF spectra measured in ranges of (c) 0–250 MHz using MH mode of ESA in  $\sim 30$  min with RBW of 51 kHz and (d) 175–225 MHz using MH mode of ESA in  $\sim 30$  min with RBW of 30 kHz. AOM: acoustic optical modulator.

Fabry-Pérot (F-P) interferometer (Thorlabs, SA200-12B) with a FSR of 1.5 GHz and a resolution of 7.5 MHz. As can be seen in Figs. 6(a)–6(d), there is only one peak captured in a FSR of 1.5 GHz for each laser, indicating the 4W-EDFL was operating in a stable SLM state at every single-wavelength lasing. To further confirm the SLM operation, we measured each laser output in turn, using the self-homodyne method with a 400 MHz PD and a radio frequency (RF) electrical spectrum

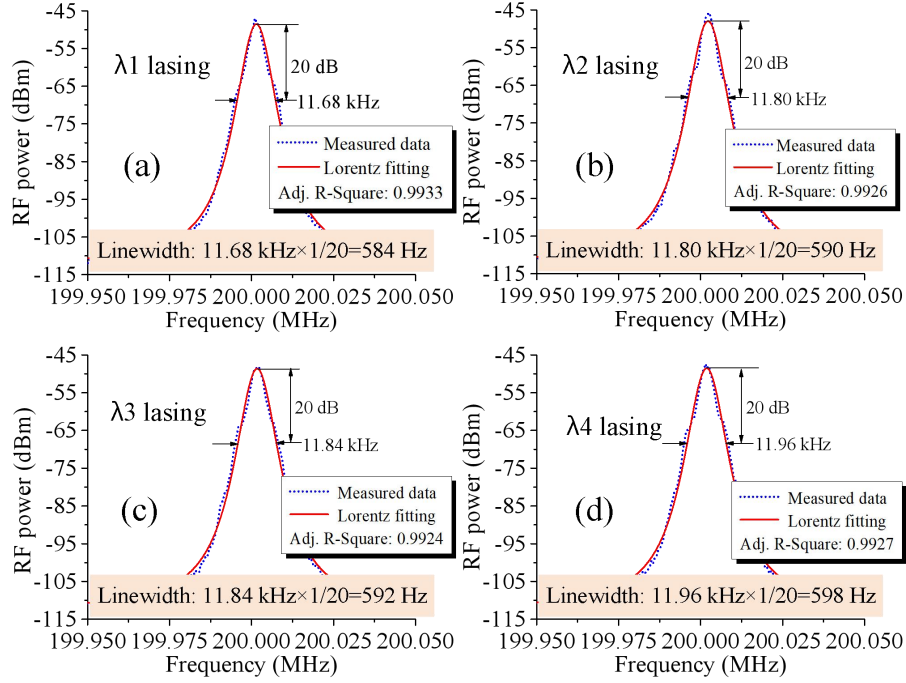


Fig. 8. Measurements of laser linewidths for all single-wavelength operations in turn using the DSHMS. Delayed self-heterodyne RF beating spectra of laser output oscillating at (a)  $\lambda_1$ , (b)  $\lambda_2$ , (c)  $\lambda_3$  and (d)  $\lambda_4$ , respectively, in 199.950~200.050 MHz using average mode (100 times) of ESA with RBW of 100 Hz. In each figure measured data fitted by Lorentz lineshape.

analyzer (ESA, Keysight N9010A), as shown in Fig. 7(a). The parameter setup of the ESA can be found in the caption of Fig. 7. As expected, in a  $\sim 10$  min measurement there is no any beating signal captured for all four lasers. In order to investigate the mode selection capability of the F8-CRC filter, we replaced it by a section of SMF to maintain the original MRC's length and then measured each laser output again using the same self-homodyne method, as shown in Fig. 7(b). Numerous spikes are seen, indicating that each laser output was with dense longitudinal-modes. In addition, the spacing of adjacent peaks is  $\sim 11.20$  MHz, which is high consistent with the calculated value of 11.17 MHz based on the measured length of MRC.

Same with that described in our previous publications [23, 24], we studied each laser's mode-hop characteristic using a delayed self-heterodyne measurement system (DSHMS) composed of the 400 MHz PD, a Mach-Zehnder interferometer (MZI) with a 200 MHz acoustic optical modulator (AOM) and 100 km long SMF in two arms respectively, and the RF ESA. In a  $\sim 30$  min measurement, the results in ranges of 0~250 MHz and 175~225 MHz are shown in Figs. 7(c) and 7(d) respectively. Due to the use of the long delay-line in the MZI and the longitudinal-mode spacing of  $\sim 11.20$  MHz, any mode-hopping could be captured, but in the figures only the strong beating signal at  $\sim 200$  MHz introduced by the AOM was captured for each laser. Therefore, we believe that our 4W-EDFL has the potential to work in a stable SLM operation at any one of the four wavelengths without mode-hop for a long time.

The linewidths of the four lasers were also measured using the DSHMS as shown in Fig. 8(a) to Fig. 8(d), with the parameter setup of ESA given in the caption of Fig. 8. The measured RF beating spectra of  $\lambda_1$ ,  $\lambda_2$ ,  $\lambda_3$  and  $\lambda_4$  lasings are all

curve-fitted well using the Lorentz lineshape, respectively with a high adjusted  $R$ -Square (Adj.  $R$ -Square) of 0.9933, 0.9926, 0.9924 and 0.9927. As marked and calculated in four graphs, the linewidths of four switchable single-wavelength lasers are 584 Hz, 590 Hz, 592 Hz and 598 Hz respectively. It is worth noting that, since we could not use a SMF delay-line over 1500 km to achieve completely incoherent mixing of two arms of the MZI theoretically due to the limitation of output laser power and serious  $1/f$  frequency noise from the ultra-long delay-line, it is impossible to obtain a pure Lorentzian linewidth spectrum. However, considering that the measured results contain the unavoidable broadening effects induced by the partial coherence mixing of MZI's two arms, the  $1/f$  frequency noise from the 100 km delay-line, we believe that the lasers' linewidths obtained must be larger than their real values. Therefore, the measured values can be regarded as conservative characterizations of the natural linewidths of our 4W-EDFL for future practical applications.

The RIN parameter is generally used to characterize the instantaneous power stability of a SLM laser. We measured the RIN spectra of four lasing wavelengths in turn using the 400 MHz PD, an oscilloscope (Tektronix, TDS2024C) and the ESA, as shown in Fig. 9(a) to Fig. 9(d), using the parameter setup of ESA as given in the caption of Fig. 9. For comparison, in each graph, the shot noise limit (SNL) for each laser is given, which can be calculated as

$$\text{SNL} = 10 \lg \left( \frac{2h\nu}{P} \right) \text{ (dB/Hz)}, \quad (16)$$

where,  $h$  is the Planck constant,  $\nu$  is the laser frequency and  $P$  is the detected laser power by the PD. As can be seen, when the

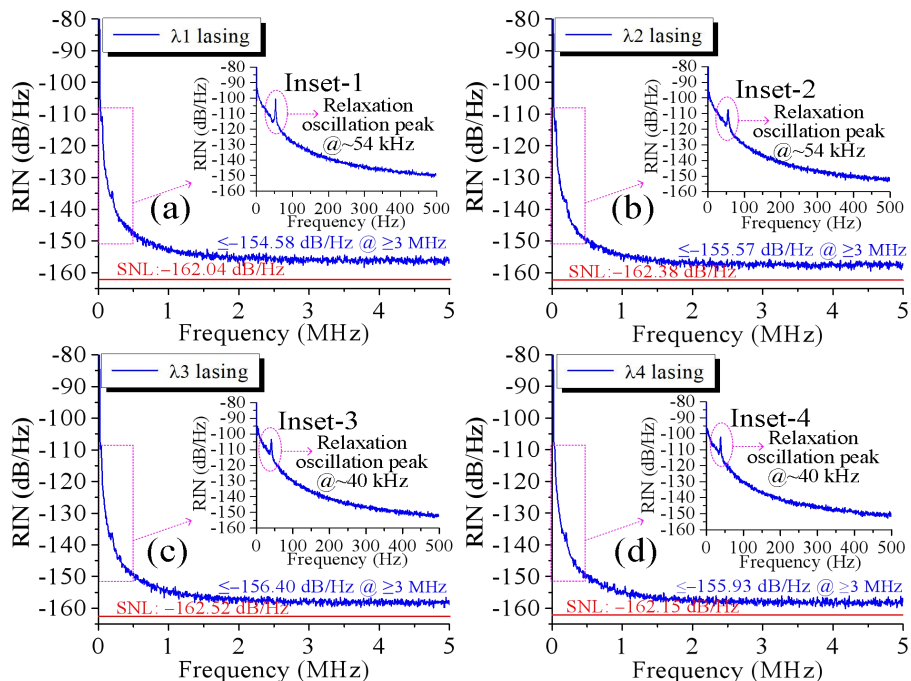


Fig. 9. RIN spectra of single-wavelength operations lasing at (a)  $\lambda_1$ , (b)  $\lambda_2$ , (c)  $\lambda_3$  and (d)  $\lambda_4$ , respectively, in 0–5 MHz using RBW of 10 kHz for ESA; for comparison, in each figure for the laser, corresponding shot-noise limit (SNL) also given and plotted; insets showing the same measurements in 0–500 kHz using RBW of 100 Hz for ESA to display the relaxation oscillation peaks.

frequency is larger than 3 MHz, the RIN of our fiber laser is  $\leq -154.58$  dB/Hz for all four output lasers, and for each laser the  $\text{RIN}@_{\geq 3}$  MHz is close to the corresponding calculated SNL. In addition, we measured the relaxation oscillation peaks for the lasers as shown in the inset of each graph. The laser's relaxation oscillation noise is mainly induced by the fluctuations of pump power and cavity loss, mechanical vibration, and thermal disturbance [56]. As can be seen, all of the peak values are  $\leq -100$  dB/Hz. The above data indicates that our 4W-EDFL has good instantaneous power stability during the measurements. Besides, we see that the relaxation oscillation frequencies of lasers  $\lambda_1$  and  $\lambda_2$  are both  $\sim 54$  kHz and lasers  $\lambda_3$  and  $\lambda_4$  are both  $\sim 40$  kHz respectively. Theoretically, a longer MRC length determines a lower relaxation oscillation frequency [14]. For our 4W-EDFL, the lasers  $\lambda_3$  and  $\lambda_4$  have longer cavity length than that of lasers  $\lambda_1$  and  $\lambda_2$ , due to the fiber separation between HB-FBG1 and HB-FBG2. Additionally, all of the relaxation oscillation frequencies are lower than that of  $\sim 60$  kHz measured in our former work [23] since in this work the MRC length is longer, which is also consistent with the theory [14].

The medium-term output power stability of the 4W-EDFL was studied by measuring the four lasers' power respectively in a 30 min time span using a power meter with a data sampling rate of 1 Hz, as shown in Fig. 10(a) to Fig. 10(d). As can be seen, the average powers are 1.422 dBm (1.387 mW), 1.911 dBm (1.553 mW), 1.384 dBm (1.375 mW) and 2.199 dBm (1.659 mW) respectively. The slight discrepancy among each other is mainly induced by the reflectivity difference of four channels of PM-FCF and the difference of net PDL losses inside the laser cavity due to the adjusting of PCs for four lasers. Furthermore, the power fluctuations are respectively marked in the graphs for

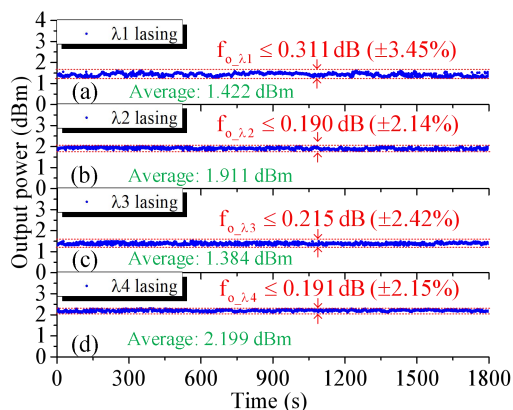


Fig. 10. Output power stabilities of single-wavelength operations lasing at (a)  $\lambda_1$ , (b)  $\lambda_2$ , (c)  $\lambda_3$  and (d)  $\lambda_4$ , respectively, measured by a laser power meter using a data sampling rate of 1 Hz in a time span of 30 min.  $f_{o,\lambda_i}$  ( $i=1, 2, 3, 4$ ): fluctuation of output power lasing at  $\lambda_i$ . The average output power for each laser also given.

four lasers. The maximum is as low as 0.311 dB ( $\pm 3.45\%$ ) at  $\lambda_1$  lasing, verifying the good power stability of our 4W-EDFL.

Polarization control is a special feature in the operation of our 4W-EDFL. Since the fiber laser cavity is not all polarization maintaining, the SOP of laser output from the pigtailed SMF jumper of OC1 cannot be guaranteed to be linear polarization, although the light reflected from any channel of the PM-FCF is linearly polarized. In order to investigate the SOP characteristics of the laser output, we measured the SOPs of four lasers in turn using a polarization analyzer (General Photonics Cor., PSY-201) as shown in Fig. 11(a) to Fig. 11(d), and each measurement was accumulated continuously for 5 min. In order to avoid the laser's SOP being influenced by the

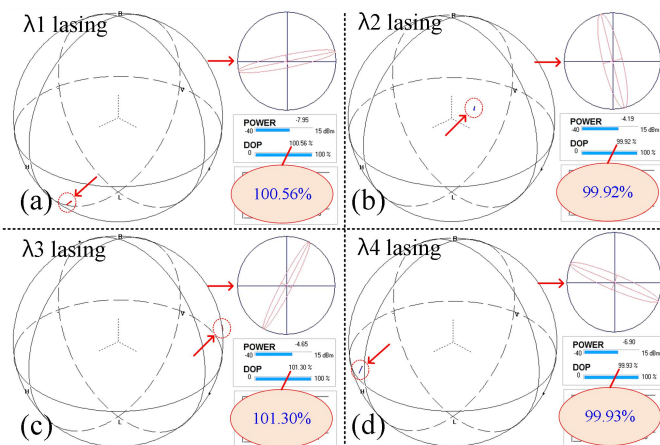


Fig. 11. SOP measurements of single-wavelength operations lasing at (a)  $\lambda_1$ , (b)  $\lambda_2$ , (c)  $\lambda_3$  and (d)  $\lambda_4$ , respectively.

instantaneous external disturbance, the output SMF jumper connecting to the PSY-201 was fixed very well using soft adhesive tapes during the measurements. As can be seen, in every image the SOP data trace on the surface of Poincaré sphere is concentrated in a small region and the degree of polarization (DOP) is close to 100% (here, the DOP values slightly larger than 100% for  $\lambda_1$  and  $\lambda_3$  lasing are induced by the analysis error of the equipment), which indicates that the SOPs of laser output for four single-wavelength operations are all with high stability and excellent single-polarization property. Additionally, from the polarization ellipse on the top-right corner of each image in Fig. 11, we see that the ellipses' major axes of lasers  $\lambda_1$  and  $\lambda_2$ /lasers  $\lambda_3$  and  $\lambda_4$  are orthogonal respectively while the ellipses' major axes of lasers  $\lambda_1$  and  $\lambda_3$ /lasers  $\lambda_2$  and  $\lambda_4$  are  $45^\circ$  with respect to each other, which is consistent with that analyzed from Fig. 2 in Section 2A.

The above performance characterizations for four lasers in single-wavelength operation of our 4W-EDFL validate that our laser system design is superior. We also believe that its output performance can be greatly improved further if a specialized packaging of vibration isolation and temperature control is employed in future for practical applications.

### B. Multi-Wavelength Operation

Based on the mechanism of  $45^\circ$  polarization-axial-offset fusion splicing between the HB-FBG1 and HB-FBG2 and the analysis on the polarization state directions of lights reflected from different channels of the PM-FCF in Section 2A, we know that there is no any two lasing wavelengths among  $\lambda_1$ ,  $\lambda_2$ ,  $\lambda_3$  and  $\lambda_4$  of the 4W-EDFL possessing the same SOP. Actually, the SOPs' major ellipse axes of any two lasers are  $45^\circ$  or an integer multiple of  $45^\circ$  with respect to each other. That can enable dual-wavelength lasing stably for our 4W-EDFL on the basis of the enhanced PHB introduced in the EDF coiled in the TL-PC. Still using the 200 mW pump power for demonstration, through adjusting the two PCs carefully, we obtained the dual-wavelength lasing at  $\lambda_1$ & $\lambda_2$ , as shown as the 3-D spectrum in Fig. 12 (a). Same with the measurement methods used for single-wavelength operation, the self-homodyne beating spectrum for demonstrating SLM lasing, the delayed

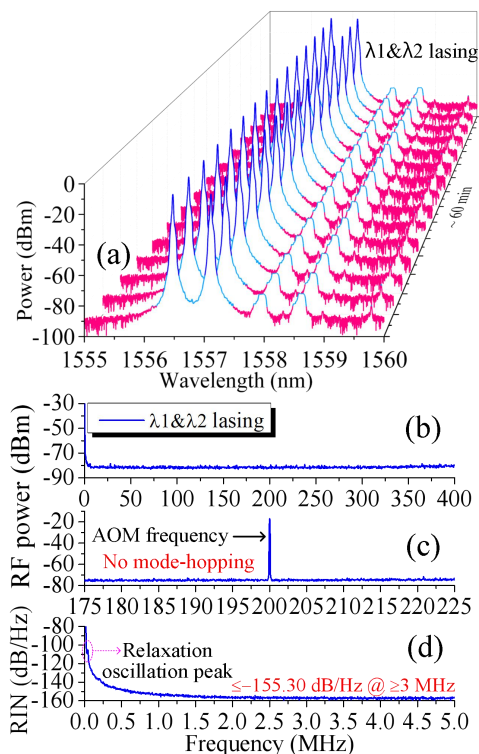


Fig. 12. Measurements of optical spectra and RF spectra in dual-wavelength operation lasing at  $\lambda_1$ & $\lambda_2$ . (a) Spectra measured by OSA for 15 repeated scans with an interval of  $\sim 4$  min; (b) Self-homodyne RF spectrum measured in a range of 0–400 MHz using maximum-hold (MH) mode of ESA in  $\sim 10$  min with resolution bandwidth (RBW) of 51 kHz; (c) Delayed self-heterodyne RF spectrum measured in a range of 0–250 MHz using MH mode of ESA in  $\sim 30$  min with RBW of 51 kHz; (d) RIN spectrum measured in 0–5 MHz using RBW of 10 kHz for ESA.

TABLE I  
PERFORMANCE PARAMETERS OF DUAL-WAVELENGTH LASING OUTPUT

Lasers <sup>a</sup>	Wavelength Fluctuation (dB)		Power Fluctuation (dB)	
$\lambda_1$ & $\lambda_2$	$f_{\lambda_1} \leq 0.005$	$f_{\lambda_2} \leq 0.006$	$f_{P1} \leq 0.851$	$f_{P2} \leq 0.952$
$\lambda_1$ & $\lambda_3$	$f_{\lambda_1} \leq 0.014$	$f_{\lambda_3} \leq 0.008$	$f_{P1} \leq 0.995$	$f_{P3} \leq 0.971$
$\lambda_1$ & $\lambda_4$	$f_{\lambda_1} \leq 0.006$	$f_{\lambda_4} \leq 0.004$	$f_{P1} \leq 0.978$	$f_{P4} \leq 0.972$
$\lambda_2$ & $\lambda_3$	$f_{\lambda_2} \leq 0.007$	$f_{\lambda_3} \leq 0.004$	$f_{P2} \leq 0.887$	$f_{P3} \leq 0.827$
$\lambda_2$ & $\lambda_4$	$f_{\lambda_2} \leq 0.011$	$f_{\lambda_4} \leq 0.010$	$f_{P2} \leq 0.960$	$f_{P4} \leq 0.883$
$\lambda_3$ & $\lambda_4$	$f_{\lambda_3} \leq 0.002$	$f_{\lambda_4} \leq 0.005$	$f_{P3} \leq 0.910$	$f_{P4} \leq 0.743$
Lasers	OSNR (dB)	SMSR (dB)	RIN (dB/Hz)	Linewidth (Hz)
$\lambda_1$ & $\lambda_2$	79	65	-155.30	
$\lambda_1$ & $\lambda_3$	78	61	-154.94	
$\lambda_1$ & $\lambda_4$	78	64	-155.41	
$\lambda_2$ & $\lambda_3$	78	62	-154.08	
$\lambda_2$ & $\lambda_4$	78	62	-154.94	
$\lambda_3$ & $\lambda_4$	78	64	-155.07	

<sup>a</sup>Note that the wavelength values of every laser in dual-wavelength operations were same with them lasing in single-wavelength operations as given in Fig. 5.

self-heterodyne spectrum for demonstrating mode-hopping free, the RIN spectrum for demonstrating high instantaneous power stability were measured for the dual-wavelength operation as shown in Fig. 12(b), (c) and (d) respectively. The parameter

TABLE II  
STABILITY COMPARISON OF DUAL-WAVELENGTH LASING BASED ON SOME  
TYPICAL TECHNIQUES

Technique	Maximal Wavelength Fluctuation	Maximal power fluctuation	Observation Time
CMFBG <sup>a</sup> + SA <sup>b</sup> [11]	N/A	1.5 dB	30 min
PM-FBG <sup>c</sup> + PM-CMFBG [22]	N/A	1.5 dB	30 min
HB-FBG + CRC [23]	0.006 nm	0.587 dB	190 min
SI-HB-FBG + CRC [24]	0.015 nm	1.348 dB	150 min
SI-FBGs + CRC [26]	0.02 nm	0.5 dB	270 min
Two BPFs <sup>d</sup> + CRC [35]	0.06 nm	1.6 dB	30 min
Structured PM-CFBG + SA [42]	0.01 nm	1 dB	N/A
Cascaded FBGs + CRC [43]	0.01 nm	2.54 dB	2.5 h
Sagnac interferometer with FBG + SA [45]	0.01 nm	3 dB	21 min
Sagnac interferometer with CFBG + SA [45]	Several pm	1 dB	20 min
<b>This work</b>	<b>0.014 nm</b>	<b>0.995</b>	<b>60 min</b>

<sup>a</sup>CM-FBG: chirped Moiré fiber Bragg grating;

<sup>b</sup>SA: saturable absorber;

<sup>c</sup>PM-FBG: polarization maintaining FBG;

<sup>d</sup>BPF: bandpass filter.

setup of instruments is given in the caption of Fig. 12. Note that since the spacing of  $\lambda_1$  and  $\lambda_2$  is  $\sim 0.67$  nm, corresponding to a frequency spacing of  $\sim 80.4$  GHz, the beating signal between  $\lambda_1$  and  $\lambda_2$  lasing cannot be detected by the 400 MHz PD used in the self-homodyne and self-heterodyne systems. As can be seen in Fig. 12, the dual-wavelength operation is with high optical spectrum and longitudinal-mode stability. The key property parameters are shown in Table I. Similarly, we also obtained other five groups of dual-wavelength combination, including  $\lambda_1$ & $\lambda_3$ ,  $\lambda_1$ & $\lambda_4$ ,  $\lambda_2$ & $\lambda_3$ ,  $\lambda_2$ & $\lambda_4$ ,  $\lambda_3$ & $\lambda_4$  lasings, all with excellent performance. For saving space we will not show more figures similar with Fig. 12, but list all of the key property parameters in Table I. As can be seen, all of the six groups of dual-wavelength operations possess extremely low wavelength and power fluctuations, high OSNRs and SMSRs, and low RINs. Especially, six dual-wavelength operations are with very similar performance, which is consistent with the expectation, benefiting from the enhanced PHB effect inside the laser cavity. Moreover, it's worth noting that all dual-wavelength operations are with the performance parameters close to those of the single-wavelength operations. The linewidth for each lasing wavelength should be measured through selecting it from two simultaneously lasing ones, using an ultra-narrowband tunable optical filter with ultra-high stopband suppression. However, we did not have such a filter, so we only directly observed the self-heterodyne beating spectra of the laser outputs of six dual-wavelength operations respectively, and the conservative linewidths mixing two lasers measured were all less than 800 Hz. In addition, in order to further prove the good performance of our 4W-EDFL, we compares the key stability parameters of dual-wavelength lasings achieved with some typical techniques, as can be seen in Table II. The data indicates that the proposed 4W-EDFL has an outstanding medium-term stability, which

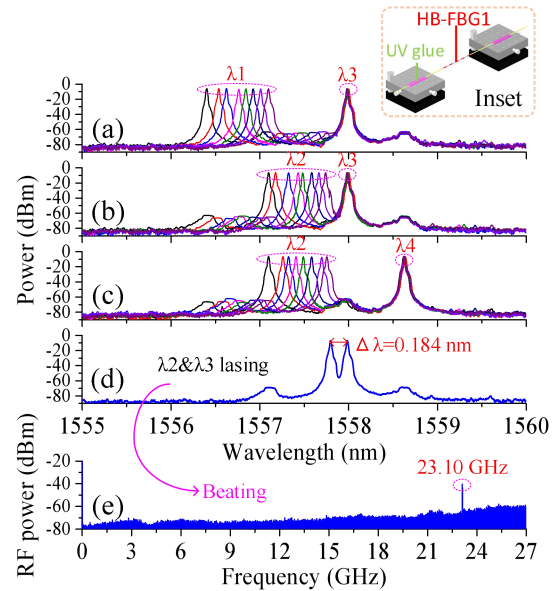


Fig. 13. Spectra of wavelength-spacing tuning for dual-wavelength operations lasing at (a)  $\lambda_1$ & $\lambda_3$ , (b)  $\lambda_2$ & $\lambda_3$  and (c)  $\lambda_2$ & $\lambda_4$ , respectively, through stretching HB-FBG1 using the setup shown in the inset. (d) Spectrum of dual-wavelength operation lasing at  $\lambda_2$ & $\lambda_3$  with a spacing of 0.184 nm; (e) Photonic generation of microwave signal at 23.10 GHz through beating the dual-wavelength lasing output shown in (d), measured by ESA and high-speed PD.

enables it to be a good switchable dual-wavelength laser source for many related important applications, especially after it is packaged by good vibration isolation and temperature control techniques.

Please note that, in experiments, the lasing state switching via adjusting the manual PCs among the six dual-wavelength operations was random, because the adjustment of PCs was not quantitative. So the only way to know which lasing state was achieved at a moment was to observe the output laser spectrum. However, by calibrating the two PCs for every lasing mode beforehand, we can also achieve to switch one operating mode to another with certainty. Or we can use the programmable PCs (for instance, the voltage-controlled PCs, which can be adjusted by the digital or analog signal) instead of the manual PCs to achieve the switching with certainty in future.

The cascading design of HB-FBG1 and HB-FBG2 makes the tuning of wavelength spacing between the two lasers in a dual-wavelength operation of the 4W-EDFL possible, which may be used to fabricate the tunable photonic generator of microwave signal. The implementation method is to stretch the HB-FBG1 with two micro-displacement platforms as shown in the inset of Fig. 13. The fiber pigtailed of the HB-FBG1 at both sides were affixed on the top-face of the platforms by the UV glue. In dual-wavelength operations lasing at  $\lambda_1$ & $\lambda_3$ ,  $\lambda_1$ & $\lambda_4$ ,  $\lambda_2$ & $\lambda_3$ , and  $\lambda_2$ & $\lambda_4$ , the wavelength spacing can be tuned when the HB-FBG1 is stretched by adjusting the micrometer of the platforms. For demonstration, Fig. 13(a) to Fig. 13(c) show the spectra of wavelength spacing tuning for  $\lambda_1$ & $\lambda_3$ ,  $\lambda_2$ & $\lambda_3$ , and  $\lambda_2$ & $\lambda_4$  lasing respectively. For demonstrating the photonic generation of microwave signal using the dual-wavelength lasing output of our 4W-EDFL, we can beat the two lasers in a high-speed PD. However, since the measureable frequency

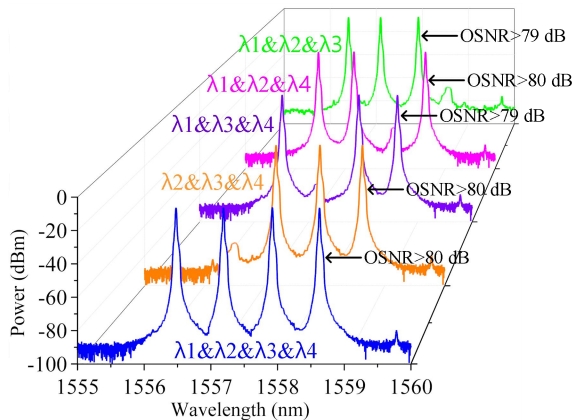


Fig. 14. Spectra of tri-wavelength operations lasing at  $\lambda_1&\lambda_2&\lambda_3$ ,  $\lambda_1&\lambda_2&\lambda_4$ ,  $\lambda_1&\lambda_3&\lambda_4$  and  $\lambda_2&\lambda_3&\lambda_4$  respectively and quad-wavelength operation lasing at  $\lambda_1&\lambda_2&\lambda_3&\lambda_4$ .

range of the ESA is 26.5 GHz, the wavelength spacing of the two lasers should be tuned to less than 0.212 nm. Fig. 13(d) shows the optical spectrum of dual-wavelength lasing at  $\lambda_2&\lambda_3$  with a spacing of 0.184 nm. By detecting the laser output with a 40 GHz PD to beat the two lasers, a microwave signal at 23.10 GHz was obtained as shown in Fig. 13(e), successfully demonstrating the feasibility and potential for photonic generation of tunable microwave signal using our 4W-EDFL.

Based on the enhanced strong PHB effect introduced by the EDF-coiled TL-PC and the  $45^\circ$  polarization-axial-offset fusion spliced PM-FCF inside the laser cavity of the 4W-EDFL, the switchable operations of power-equalized tri-wavelength and quad-wavelength lasing were also achieved through adjusting the PCs carefully. Figure 14 shows the typical spectra of four tri-wavelength operations respectively lasing at  $\lambda_1&\lambda_2&\lambda_3$ ,  $\lambda_1&\lambda_2&\lambda_4$ ,  $\lambda_1&\lambda_3&\lambda_4$  and  $\lambda_2&\lambda_3&\lambda_4$ , and the typical spectrum of the four-wavelength operation. As marked in the figure, the OSNR is  $>79$  dB for all of the operations, indicating that the 4W-EDFL was still with excellent output performance in multi-wavelength operations. Similar with the demonstration in our previous work [24], the switching among five multi-wavelength operations was harder than that among four single- and six dual-wavelength operations for this 4W-EDFL. However, the switching difficulty was significantly lower than that in [24]. We believe that must benefit from the specially enhanced PHB effect by the PM-FCF. Since the tri- or quad-wavelength operation is not the emphasis here, we will not show more characterizations for saving space.

#### IV. CONCLUSION

We have reported what we believe to be the first 4W-EDFL enabled by a F8-CRC filter for SLM selection and a PM-FCF for defining lasing wavelengths. The F8-CRC filter is simply made of three OCs with extremely low cost and high filtering capability. The PM-FCF is structured by two HB-FBGs fusion-spliced together with a  $45^\circ$  polarization-axial-offset. We introduce a novel methodology utilizing the signal-flow graph combined with the Mason's rule to theoretically analyze a CRC filter in general, and apply it to obtain the important design

parameters for the F8-CRC filter used in the proposed 4W-EDFL. This method can be a common approach for designing, fabricating and characterizing CRC filters aiming for applying in SLM fiber lasers. The measured transmission spectrum of the fabricated F8-CRC filter is highly consistent with the simulated result. By integrating the F8-CRC filter and the PM-FCF in a fiber laser theoretical model, we validate that the SLM lasing can be achieved in each channel of the PM-FCF. Due to the use of the PM-FCF, the polarization ellipses' major axes of any two lasing wavelengths are  $45^\circ$  or an integer multiple of  $45^\circ$  with respect to each other. In addition, the PHB effect in the EDF coiled in the TL-PC is significantly enhanced, compared to that in our previous work [24]. By adjusting the two PCs, the switching among fifteen lasing states was experimentally validated, including four single-, six dual-, four tri- and one quad-wavelength operations. In single-wavelength operations, the four lasing outputs are all in stable SLM oscillation, typically with a linewidth of  $<600$  Hz, a RIN of  $\leq -154.58$  dB/Hz@ $\geq 3$  MHz and an output power fluctuation of  $\pm 3.45\%$ . In dual-wavelength operations, the two lasing wavelengths of all output states have very similar performance, also with the performance parameters close to those of single-wavelength operations. In addition, the switching among tri- and quad-wavelength operations is much easier than that in [24], which is validated during the experiments. We also demonstrate the wavelength spacing adjustment of the dual-wavelength operations, which can be used for photonic generation of tunable microwave signals, and obtain a 23.10 GHz signal successfully by beating the dual-wavelength lasing with a spacing of 0.184 nm. We believe that the outstanding performances of our 4W-EDFL can be further improved if special temperature compensation and vibration isolation are employed in future for practical applications.

#### REFERENCES

- [1] N. Cezard, *et al.*, "Performance assessment of a coherent DIAL-Doppler fiber lidar at 1645 nm for remote sensing of methane and wind," *Opt. Express*, vol. 28, no. 15, pp. 22345-22357, Jul. 2020.
- [2] J. Qin, *et al.*, "Ultra-long range optical frequency domain reflectometry using a coherence-enhanced highly linear frequency-swept fiber laser source," *Opt. Express*, vol. 27, no. 14, pp. 19359-19368, Jul. 2019.
- [3] H. Al-Taiy, N. Wenzel, S. Preußler, J. Klinger, and T. Schneider, "Ultra-narrow linewidth, stable and tunable laser source for optical communication systems and spectroscopy," *Opt. Lett.*, vol. 39, no. 20, pp. 5826-5829, Oct. 2014.
- [4] T. Omiya, M. Yoshida, and M. Nakazawa, "400 Gbit/s 256 QAM-OFDM transmission over 720 km with a 14 bit/s/Hz spectral efficiency by using high-resolution FDE," *Opt. Express*, vol. 21, no. 3, pp. 2632-2641, Feb. 2013.
- [5] Y. Fei, *et al.*, "100-mW linear polarization single-frequency all-fiber seed laser for coherent Doppler lidar application," *Opt. Commun.*, vol. 285, no. 2, pp. 149-152, Jan. 2012.
- [6] H. Katori, "Optical lattice clocks and quantum metrology," *Nat. Photonics*, vol. 5, no. pp. 203-210, Mar. 2011.
- [7] C. W. Chou, D. B. Hume, T. Rosenband, and D. J. Wineland, "Optical clocks and relativity," *Science*, vol. 329, no. 5999, pp. 1630-1633, Sep. 2010.
- [8] C. Sun, Y. Dong, M. Wang, and S. Jian, "Liquid level and temperature sensing by using dual-wavelength fiber laser based on multimode interferometer and FBG in parallel," *Opt. Fiber Technol.*, vol. 41, pp. 212-216, Mar. 2018.

- [9] T. Sun, Y. Guo, T. Wang, J. Huo, and L. Zhang, "Dual-wavelength single longitudinal mode fiber laser for microwave generation," *Opt. Laser Technol.*, vol. 67, pp. 143-145, Apr. 2015.
- [10] J. Zhou, X. Feng, Y. Wang, Z. Li, and B.-O. Guan, "Dual-wavelength single-frequency fiber laser based on FP-LD injection locking for millimeter-wave generation," *Opt. Laser Technol.*, vol. 64, pp. 328-332, Jun. 2014.
- [11] S. Feng, *et al.*, "Photonic generation of microwave signal using a dual-wavelength erbium-doped fiber ring laser with CMFBG filter and saturable absorber," *Opt. Laser Technol.*, vol. 45, no. 1, pp. 342-347, Aug. 2013.
- [12] P. Bakopoulos, *et al.*, "Multi-wavelength laser source for dense wavelength division multiplexing networks," in *Optical Fiber Communication Conference and Exposition and The National Fiber Optic Engineers Conference*, Anaheim, California, 2007, p. OWJ2.
- [13] S. Mo, *et al.*, "600-Hz linewidth short-linear-cavity fiber laser," *Opt. Lett.*, vol. 39, no. 20, pp. 5818-5821, Oct. 2014.
- [14] S. Mo, *et al.*, "820 Hz linewidth short-linear-cavity single-frequency fiber laser at 1.5  $\mu\text{m}$ ," *Laser Phys. Lett.*, vol. 11, no. 3, Jan. 2014, Art. no. 035101.
- [15] W. Zhang, *et al.*, "A compact low noise single frequency linearly polarized DBR fiber laser at 1550 nm," *Chin. Opt. Lett.*, vol. 29, no. 8, Jul. 2012, Art. no. 084205.
- [16] Q. Li, *et al.*, "DFB laser based on single mode large effective area heavy concentration EDF," *Opt. Express*, vol. 20, no. 21, pp. 23684-23689, Oct. 2012.
- [17] Q. Li, *et al.*, "A single frequency, linear cavity Tm-doped fiber laser based on phase-shifted FBG filter," *Opt. Laser Technol.*, vol. 56, pp. 304-306, Sep. 2014.
- [18] Y. Zhao, *et al.*, "Research on a novel composite structure Er<sup>3+</sup>-doped DBR fiber laser with a  $\pi$ -phase shifted FBG," *Opt. Express*, vol. 21, no. 19, pp. 22515-22522, Sep. 2013.
- [19] X. Wang, T. Zhu, L. Chen, and X. Bao, "Tunable Fabry-Perot filter using hollow-core photonic bandgap fiber and micro-fiber for a narrow-linewidth laser," *Opt. Express*, vol. 19, no. 10, pp. 9617-9625, May 2011.
- [20] X. Chen, J. Yao, Z. Fei, and Z. Deng, "Single-longitudinal-mode fiber ring laser employing an equivalent phase-shifted fiber Bragg grating," *IEEE Photon. Technol. Lett.*, vol. 17, no. 7, pp. 1390-1392, Jul. 2005.
- [21] X. P. Cheng, *et al.*, "Single-longitudinal-mode erbium-doped fiber ring laser based on high finesse fiber Bragg grating Fabry-Pérot etalon," *IEEE Photon. Technol. Lett.*, vol. 20, no. 12, pp. 976-978, Jun. 2008.
- [22] B. Yin, S. Feng, Z. Liu, Y. Bai, and S. Jian, "Tunable and switchable dual-wavelength single polarization narrow linewidth SLM erbium-doped fiber laser based on a PM-CMFBG filter," *Opt. Express*, vol. 22, no. 19, pp. 22528-22533, Sep. 2014.
- [23] T. Feng, M. Wang, X. Wang, F. Yan, Y. Suo, and X. S. Yao, "Switchable 0.612-nm-spaced dual-wavelength fiber laser with sub-kHz linewidth, ultra-high OSNR, ultra-Low RIN, and orthogonal polarization outputs," *J. Lightwave Technol.*, vol. 37, no. 13, pp. 3173-3182, Jul. 2019.
- [24] T. Feng, *et al.*, "Four-wavelength-switchable SLM fiber laser with sub-kHz linewidth using superimposed high-birefringence FBG and dual-coupler ring based compound-cavity filter," *Opt. Express*, vol. 27, no. 25, pp. 36662-36679, Dec. 2019.
- [25] T. Feng, D. Ding, Z. Zhao, H. Su, F. Yan, and X. S. Yao, "Switchable 10 nm-spaced dual-wavelength SLM fiber laser with sub-kHz linewidth and high OSNR using a novel multiple-ring configuration," *Laser Phys. Lett.*, vol. 13, no. 10, Aug. 2016, Art. no. 105104.
- [26] T. Feng, D. Ding, F. Yan, Z. Zhao, H. Su, and X. S. Yao, "Widely tunable single-/dual-wavelength fiber lasers with ultra-narrow linewidth and high OSNR using high quality passive subring cavity and novel tuning method," *Opt. Express*, vol. 24, no. 17, pp. 19760-19768, Aug. 2016.
- [27] L. Tang, J. Shang, Z. Wang, K. Mu, Y. Qiao, and S. Yu, "Gourd-shaped subring resonator-based single longitudinal mode erbium-doped fiber laser," *Opt. Eng.*, vol. 58, no. 6, Jun. 2019, Art. no. 066110.
- [28] L. Li, M. Zhang, Y. Liu, Y. Li, and Y. Wang, "Stable single-longitudinal-mode erbium-doped fiber laser with narrow linewidth utilizing parallel fiber ring resonator incorporating saturable absorber and fiber Bragg grating," *Appl. Opt.*, vol. 54, no. 13, pp. 4001-4005, May 2015.
- [29] S. Feng, Q. Mao, Y. Tian, Y. Ma, W. Li, and L. Wei, "Widely tunable single longitudinal mode fiber laser with cascaded fiber-ring secondary cavity," *IEEE Photon. Technol. Lett.*, vol. 25, no. 4, pp. 323-326, Feb. 2013.
- [30] W. Li and J. Sun, "Optical vernier filter with cascaded double-coupler compound fiber loop resonators," *Optik*, vol. 121, no. 15, pp. 1370-1375, Sep. 2010.
- [31] Y. Li, Y. Shen, J. Tian, Q. Fu, and Y. Yao, "Wavelength switchable multi-wavelength erbium-doped fiber laser based on polarization-dependent loss modulation," *J. Lightwave Technol.*, vol. 39, no. 1, pp. 243-250, Jan. 2021.
- [32] Q. Zhao, *et al.*, "Switchable multi-wavelength erbium-doped fiber laser with adjustable wavelength interval," *J. Lightwave Technol.*, vol. 37, no. 15, pp. 3784-3790, Aug. 2019.
- [33] T. Feng, *et al.*, "C-band 41-wavelength-switchable single-longitudinal-mode fiber laser with sub-kHz linewidth and high stability using a wide-band chirped Moiré fiber Bragg grating," *Laser Phys. Lett.*, vol. 16, no. 2, Jan. 2019, Art. no. 025106.
- [34] Y. Qi, *et al.*, "Wavelength-switchable fiber laser based on few-mode fiber filter with core-offset structure," *Opt. Laser Technol.*, vol. 81, pp. 26-32, Jan. 2016.
- [35] C.-H. Yeh, J.-Y. Chen, H.-Z. Chen, and C.-W. Chow, "Selectable dual-wavelength erbium-doped fiber laser with stable single-longitudinal-mode utilizing eye-type compound-ring configuration," *Opt. Laser Technol.*, vol. 82, pp. 72-75, Aug. 2016.
- [36] R. A. Pérez-Herrera, L. Rodríguez-Cobo, M. A. Quintela, J. M. L. Higuera, and M. López-Amo, "Single-longitudinal-mode dual wavelength-switchable fiber laser based on superposed fiber Bragg gratings," *IEEE Photon. Journal*, vol. 7, no. 2, Apr. 2015, Art. no. 7101307.
- [37] A. A. Jasim, M. Dernaika, S. W. Harun, and H. Ahmad, "A switchable figure eight erbium-doped fiber laser based on inter-modal beating by means of non-adiabatic microfiber," *J. Lightwave Technol.*, vol. 33, no. 2, pp. 528-534, Jan. 2015.
- [38] W. He and L. Zhu, "Switchable dual-wavelength single-longitudinal-mode erbium-doped fiber laser based on a thin-core fiber comb filter and saturable absorber," *Microwave Opt. Technol. Lett.*, vol. 57, no. 2, pp. 287-92, Feb. 2015.
- [39] K. K. Qureshi, "Switchable dual-wavelength fiber ring laser featuring twin-core photonic crystal fiber-based filter," *Chin. Opt. Lett.*, vol. 12, no. 2, Feb. 2014, Art. no. 020605.
- [40] T. Feng, F. Yan, S. Liu, Y. Bai, W. Peng, and S. Tan, "Switchable and tunable dual-wavelength single-longitudinal-mode erbium-doped fiber laser with special subring-cavity and superimposed fiber Bragg gratings," *Laser Phys. Lett.*, vol. 11, no. 12, Nov. 2014, Art. no. 125106.
- [41] Z. Cao, *et al.*, "Switchable dual-wavelength erbium-doped fiber ring laser with tunable wavelength spacing based on a compact fiber filter," *Opt. Laser Technol.*, vol. 56, pp. 137-141, Mar. 2014.
- [42] B. Yin, *et al.*, "Switchable single-polarization dual-wavelength ring laser based on structured PM-CFBG," *IEEE Photon. Technol. Lett.*, vol. 26, no. 12, pp. 1227-1230, Jun. 2014.
- [43] T. Feng, *et al.*, "A switchable and wavelength-spacing tunable single-frequency and single-polarization dual-wavelength erbium-doped fiber laser based on a compound-cavity structure," *Laser Phys.*, vol. 24, no. 8, Jun. 2014, Art. no. 085101.
- [44] C. Zhang, J. Sun, and S. Jian, "A new mechanism to suppress the homogeneous gain broadening for stable multi-wavelength erbium-doped fiber laser," *Opt. Commun.*, vol. 288, pp. 97-100, Oct. 2013.
- [45] X. Y. He, D. N. Wang, and C. R. Liao, "Tunable and switchable dual-wavelength single-longitudinal-mode erbium-doped fiber lasers," *J. Lightwave Technol.*, vol. 29, no. 6, pp. 842-849, 4 Mar. 2011.
- [46] W. Zheng, S. Ruan, M. Zhang, W. Liu, Y. Zhang, and X. Yang, "Switchable multi-wavelength erbium-doped photonic crystal fiber laser based on nonlinear polarization rotation," *Opt. Laser Technol.*, vol. 50, pp. 145-149, Apr. 2013.
- [47] W. Peng, F. Yan, Q. Li, S. Liu, T. Feng, and S. Tan, "A 1.97  $\mu\text{m}$  multiwavelength thulium-doped silica fiber laser based on a nonlinear amplifier loop mirror," *Laser Phys. Lett.*, vol. 10, no. 11, Sep. 2013, Art. no. 115102.
- [48] Q. Zhao, *et al.*, "Switchable multi-wavelength erbium-doped fiber laser based on core-offset structure and four-wave-mixing effect," *Opt. Fiber Technol.*, vol. 54, Jan. 2020, Art. no. 102111.
- [49] S. W. Harun, R. Parvizi, S. Shahi, and H. Ahmad, "Multi-wavelength erbium-doped fiber laser assisted by four-wave mixing effect," *Laser Phys. Lett.*, vol. 6, no. 11, pp. 813-815, Nov. 2009.
- [50] X. M. Liu, "Four-wave mixing self-stability based on photonic crystal fiber and its applications on erbium-doped fiber lasers," *Opt. Commun.*, vol. 260, no. 2, pp. 554-559, Apr. 2006.

- [51] Z. Chun-Liu, *et al.*, “Switchable multi-wavelength erbium-doped fiber lasers by using cascaded fiber Bragg gratings written in high birefringence fiber,” *Opt. Commun.*, vol. 230, no. 4, pp. 313-317, Feb. 2004.
- [52] K. O. Hill, B. Malo, F. Bilodeau, D. C. Johnson, and J. Albert, “Bragg gratings fabricated in monomode photosensitive optical fiber by UV exposure through a phase mask,” *Appl. Phys. Lett.*, vol. 62, no. 10, pp. 1035-1037, Mar. 1993.
- [53] L. N. Binh, S. F. Luk, and N. Q. Ngo, “Amplified double-coupler double-ring optical resonators with negative optical gain,” *Appl. Opt.*, vol. 34, no. 27, pp. 6086-6094, Sep. 1995.
- [54] S. J. Mason, “Feedback theory—further properties of signal flow graphs,” *Proceedings of the IRE*, vol. 44, no. 7, pp. 920-926, Feb. 1956.
- [55] V. J. Mazurczyk and J. L. Zyskind, “Polarization dependent gain in erbium doped-fiber amplifiers,” *IEEE Photon. Technol. Lett.*, vol. 6, no. 5, pp. 616-618, May. 1994.
- [56] T. Tan, *et al.*, “Ultralow-intensity-noise single-frequency fiber-based laser at 780 nm,” *Applied Physics Express*, vol. 13, no. 2, Jan. 2020, Art. no. 022002.

**Ting Feng** received the Ph.D. degree in communication and information system from the Key Laboratory of All Optical Network and Advanced Telecommunication Network, Ministry of Education, Beijing Jiaotong University, Beijing, China, in January 2015.

From September 2012 to September 2013, he was a Visiting Scholar with the Optics Laboratory, School of Electrical and Computer Engineering, Georgia Institute of Technology, Atlanta, GA, USA. He joined the Photonics Information Innovation Center, College of Physics Science and Technology, Hebei University, Baoding, China, in 2015, where he was promoted as an Associate Professor, in 2016. In 2020, he was promoted as an outstanding young scholar of Hebei province and a Hebei new century “333 talent project” suitable person. He is a member of the Optical Society of America (OSA) and a member of the Chinese Optical Society (COS). He has chaired and participated in more than ten research projects funded by the National Nature Science Foundation of China, Natural Science Foundation of Hebei Province, *et al.* He has authored more than 90 refereed journal articles, written two optics related books, and been granted with more than 30 patents in related areas. His research interests include optical fiber lasers, optical fiber sensing, and their application technologies.

**Da Wei**, biography not available.

**Wenwen Bi**, biography not available.

**Weiwei Sun**, biography not available.

**Shengbao Wu**, biography not available.

**Meili Jiang**, biography not available.

**Fengping Yan**, biography not available.

**Yuping Suo**, biography not available.

**X. Steve Yao** (M’97—F’18) received the M.S. and Ph.D. degrees in electrical engineering/electrophysics from the University of Southern California, Los Angeles, CA, USA, in 1989 and 1992, respectively.

He was the Chief Technology Officer of General Photonics Corporation and now holds the Changjiang Scholar

Professorship with the Hebei University, Baoding, China. He has authored more than 90 referred journal publications, been granted with more than 75 U.S. patents, given invited speeches in numerous major photonics-related conferences, and authored three book chapters. From 1990 to 2000, he was with NASA’s Jet Propulsion Laboratory (JPL), responsible for the design and demonstration of the X-band fiber optic antenna remoting system for NASA’s Deep Space Network. Prior to JPL, from 1985 to 1987, he was an Optical Engineer with ADC fiber Optics (a division of the ADC Telecommunications), responsible for developing the first generation of fiber optic wavelength division multiplexing (WDM) devices. He is a Fellow of IEEE, a Fellow of OSA, was a Topical Editor of Optics Letters, and served as a Member of the Technical Committee in the Optical Fiber Communications conferences in 1998, 2000, 2001, as the President of the Photonics Society of Chinese Americans (PSC) in 2011. Several products based on his inventions have won multiple industrial awards, including Photonics Circle of Excellence Awards, Laser Focus Innovative Product Awards, and SPIE Prism Awards. He was the recipient of 29 NASA’s innovation awards.